Journal of Materials Chemistry A

Accepted Manuscript

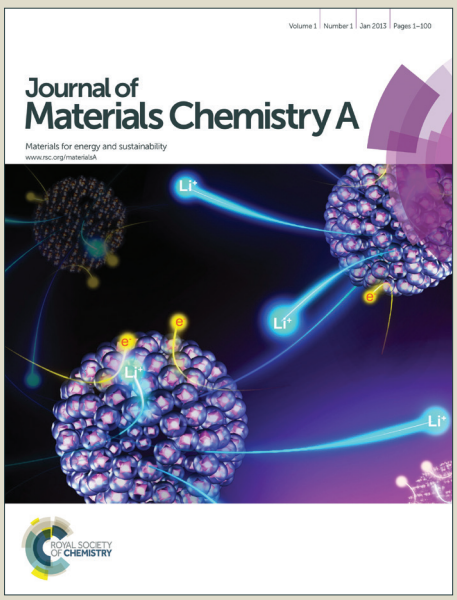

ROYAL SOCIETY OF CHEMISTRY

www.rsc.org/materialsA

Journal of Materials Chemistry A

ARTICLE

Bio-process Inspired Synthesis of Hierarchically Porous Nitrogen-doped TiO_2 with High Visible-light Photocatalytic Activity

Received 00th June 2015,
Accepted 00th August 2015

DOI: 10.1039/x0xx00000x

www.rsc.org/

Hui Zeng,[a] Jingjing Xie,[a] Hao Xie,[b] Bao-Lian Su,[a,c] Menghu Wang,[a] Hang Ping [a], Weimin Wang,[a] Hao Wang,[a] Zhengyi Fu*[a]

Inspired by structure-forming process of biominerals, scientists have made successes in synthesizing materials with elegant structures by using organic matrices as templates. However, there are still issues in relating to the exquisiteness and complexity of natural organic matrices in living organisms, which have kept its activities out of the chemists' control, especially on the functional properties of materials. Here we employ natural assorted proteins, which derived from extrapallial fluid in living mussels, to synthesize hierarchically porous nitrogen-doped TiO_2 in a singel process. The silk-like organic residuals in powders clearly show that the proteins act as the segmentation space for TiO_2 nucleation. We also demonstrate phase control over the material, with the ability to synthesize pure anatase. Synthetic TiO_2 materials show an significant improvement on the visible-light photocatalytic activity both on the degradation of organic pollutions and hydrogen production. The degradation of RhB could be almost completed in just 20 min. The visible-light photocatalytic activities vary with the concentations of EPF proteins, and the optimal concentration of protein was found to be 600 μg/ml. The present work highlights its potential application of natural organic matrix in producing advanced materials with optimized functional properties.

1. Introduction

Biomineralization is an environmentally friendly process that can fabricate biominerals with well-defined structures and optimized properties at ambient temperature,[1-4] in contrast to our present technological world where harsh conditions are commonly prerequisites.[5-7] Learning from the process of biominerals formation provides tremendous ideas for developing new synthesis technology, which can be referred as bio-process inspired synthesis. It has been found that organic matrices especially proteins play fundamental roles in biomineralization.[8-10] Therefore, so far, the bio-process inspired synthesis mainly focused on the using of organic matrices which act as "structure-directing agents" and/or "process-directing agents" to control the nucleation, growth and morphology of inorganic materials.[10-12] In most situations, owing to the exquisite and complex components, which is under rigid regulation of living system, the natural proteins in living system usually still exhibit higher efficiency in promoting minerals formation, as compared with single proteins or synthetic analogues.[11,13] Recently, the biomineralization process has also been utilized to prepare functional materials used in areas of high-temperature superconductivity, photocatalysis, lithium-ion batteries and so on.[14-16] Nevertheless, limited reports have focused on adopting fresh natural protein-assisted strategies in improving the functional properties of materials.

Titanium dioxide (TiO_2) is one of the most widely investigated photocatalyst materials with broad applications[17-19] to facilitate solving simultaneously the incoming energy and environmental problems. TiO_2 can only absorbs UV light due to its inherent large band gap (3.2 eV).[20] Several attempts are undertaken to narrow its band gap or form interstitial gap to improve the visible-light efficiency.[20-23] In particular, a variety of nitrogen sources, including NH_3 flow,[20] urea[24,25] organic amine,[26,27] ammonium hydroxide[28,29] and guanidine carbonate[30] were explored to synthesize nitrogen-doped TiO_2 (N-TiO_2) nanocrystals to improve the visible-light photocatalytic activity. On the other hand, an effective strategy to enhance photocatalytic activity is the introduction of hierarchical porosity into TiO_2.[31-33] Thus, some work has been reported on the preparation of hierarchically porous N-TiO_2 materials.[24-26] For example, Wang et. al has successfully fabricated hierarchically meso-/macroporous N-TiO_2 with visible-light photocatalytic activity.[26] However, high temperature and/or complicated preparation process, which limits its practical use. Therefore, an ideal synthetic method for controlling microstructure, crystal phase, light-use efficiency of N-TiO_2 in a single process, especially at low temperature, still constitutes a major challenge.[15,34]

Natural extrapallial fluid (EPF) proteins, a composite protein in living mussels are responsible for the formation of oriented aragonite-calcium carbonate ($CaCO_3$). During the $CaCO_3$ biomineralization, the EFP proteins exhibit improved mineral-forming activities owing to the synergic effects between different proteins. In addition to excellent structure of "brick and mortar", unique interactions between the organic matrices and inorganic matters also make aragonite far superior to current artificial $CaCO_3$ in terms of mechanical

properties.[35] However, whether Living EPF proteins could regulate the functional properties of abiological materials, is still a question.

In the present work, a simple yet efficient "one-pot" method was developed to synthesize hierarchically Porous N-TiO_2 nanocrystals at a low temperature. The obtained N-TiO_2 exhibits significantly enhanced visible-light photocatalytic activity on degradation of pollutions and hydrogen production. Moreover, mysterious relations between natural living proteins and functional properties of materials have been uncovered.

2. Experimental

2.1 Extraction of extrapallial fluid proteins

Fresh water mussels (*Cristaria plicata*) were purchased from Shao He Pear Company of Zhanjiang, Guang Dong province, China, and were maintained in glass aquariums filled with aerated oxygen for 2 days prior to experiment. Extrapallial fluid was collected by inserting a Rannin into the central extrapallial space and sucking the viscous fluid gently. The Rannin tip was carefully kept in contact with the inner shell surface to avoid contamination by extraneous water or other body fluids. Isolated fluid was immediately transferred to sterile centrifuge tubes and held on ice. The composite extrapallial fluid proteins were analyzed and visualized with Coomassie blue stained SDS-PAGE (sodium dodecyl sulfate polyacrylamide gel electrophoresis). Protein amount was determined with Bradford assay, and then the EPF proteins were diluted or concentrated to the desired concentration.

2.2 Synthesis of TiO_2 materials

Hierarchically porous nitrogen-doped TiO_2 were synthesized by a bio-process inspired method of using EPF proteins as both organic template and nitrogen source. Typically, 5 ml of EFP proteins at various concentrations were dropped into 1 ml of tetrabutyl titanate (TBT, 97%, Sigma Aldrich) under stirring for 2 h. Mineralization was allowed in the mixtures at room temperature for 4 h. After mineralization, the mixture was transferred into a Teflon-lined autoclave and pre-heated at 50 °C for 30 min. Then the temperature was raised up to 150 °C with a heating rate of 5 °C /min and kept at 150 °C for 12 h to sufficiently complete the reaction. After the reactor was naturally cooled to room temperature, the obtained brown TiO_2 powders were filtered, washed, dried, and denoted as MNT with protein concentration indicated. For example, when the concentration of composite protein was 600 μg/ml, the obtained TiO_2 was denoted as MNT-600. Pure water instead of EPE proteins was used as solvent, and the product was denoted as pristine TiO_2. As-synthesized TiO_2 prepared by Bovine serum albumin instead of EPE proteins was denoted as BSA-TiO_2 and used as a reference. The commonly used commercial P25 was also used as another reference.

We also investigated the functions of EPF proteins extracted from the same species of mussels (*Cristaria plicata*), but just lived in different original areas. The other two EPF proteins were extracted from mussels, which lived in Shantou city, Fujian province and Wuhan city, Hubei province of China, respectively. The as-synthesized sample was denoted as MNT-600-A and MNT-600-B, respectively.

2.3 Characterization of materials

The morphology of TiO_2 samples was characterized by scanning electron microscopy (FESEM, Hitachi 4800), transmission electron microscopy (TEM, JEM-2010 HT). The crystalline phase was determined by X-ray diffraction (XRD, PANalytical X'Pert Pro X-ray diffraction Cu Ka). Nitrogen adsorption-desorption isotherms were collected at -196 °C over a wide relative pressure ranging from 0.01 to 0.995 with a volumetric adsorption analyzer (ASAP-2020M). The pore diameter and pore size distribution were determined by the Barret-Joyner-Halenda (BJH) method. XPS analysis was conducted to verify the states and species of elements through an X-ray photoelectron spectrometer (VG Multilab 2000). The UV-vis absorption spectra of samples were measured on the integrating sphere (UV-2550, Shimadzu, Japan) over the wavelength range from 200 to 800 nm, and $BaSO_4$ was used as a reflectance standard.

2.4 Photocatalytic dye degradation

The photocatalytic activity of sample was investigated by dye degradation under visible-light irradiation. A 350 W xenon lamp with a UV-cutoff filter (providing visible-light with $\geq$ 420 nm) was used as a light source. Experimental details are as follows: 20 mg of TiO_2 powders were dispersed into 20 ml of 0.01 mM Rhodamine B (RhB) aqueous solution. The solution was allowed to reach an adsorption-desorption equilibrium among the photocatalyst, RhB, and water before irradiation. A ca. 2 ml aliquot was taken at regular intervals and centrifuged at 10000 rpm for 5 min to completely remove the suspended TiO_2 nanocrystals. The concentration was determined using UV-vis adsorption spectrum measurements. Furthermore, using the same procedure, the photocatalytic activity of samples for decomposition of 1 mM phenol was also investigated.

2.5 Photocatalytic hydrogen production

The photocatalytic hydrogen production experiments were performed in a 100 mL Pyrex round-bottom flask. A 350 W xenon arc lamp with a UV-cutoff filter (providing visible-light with $\geq$ 420 nm) was used as a visible-light source to trigger the photocatalytic reaction. It was measured on an FZ-A visible-light radiometer (made in the photoelectric instrument factory of Beijing Normal University, China) over the wavelength in the range of 400-1000 nm. In a typical photocatalytic experiment, 50 mg of TiO_2 photocatalyst was dispersed with in an 80 mL mixed solution of methanol (20 mL) and water (60 mL) at constant stirring. The loading of 0.6 wt % Pt cocatalyst was

added by directly dissolving H_2PtCl_6 into the above mixed solution using a photochemical reduction deposition method. Prior to irradiation, the system was bubbled with nitrogen for 40 min to remove the dissolved oxygen and to ensure the anaerobic conditions in the reaction system. A 0.4 mL sample of the generated gas was collected intermittently through the septum, and hydrogen was analyzed by gas chromatograph (GC-14C, Shimadzu, Japan, TCD, nitrogen as a carrier gas and 5 Å molecular). All glassware was cleaned and carefully rinsed with distilled water prior to use.

3. Results and discussion

The components of EFP proteins were confirmed by SDS-PAGE, revealing that various kinds of proteins are indeed in extrapallial fluid (Fig. 1a). During the $CaCO_3$ biomineralization, the EFP proteins exhibit improved mineral-forming activities, owing to the synergic effects between these different proteins. In the present work, TiO_2 formation in the presence of EFP proteins were explored and compared to that without protein. Without any additive, nanospherical TiO_2 particles are formed (Fig. 1b) as expected. In contrast, 3D Network structured TiO_2 is achieved by the mineralization of TBT in EFP proteins. The morphologies of MNT samples were characterized by scanning electron microscopy (Fig. 1c-f). It is clear that the porous TiO_2 network is constructed by nanocrystals building units, and the morphologies vary with the concentrations of EPF proteins. With the 300 μg/ml EPF proteins, although some macropores are formed, the diameter of macropore is much smaller than those at high concentrations (Fig. 1c). Fig. 1d demonstrates that the MNT-600 sample exhibits relatively homogeneous and long-range periodical pores with diameters of 200~500 nm and pore-wall thicknesses of 100~200 nm. The pore-wall is apparently built from tiny nanocrystals subunits. However, when the protein concentration continues to increase, some silk-like organic residuals are observed in the MNT-900 powders (Fig. 1e). As shown in Fig. 1f, it is noticeable that the assembled organic matrix (red arrowheads) provides a framework for TiO_2 formation. The proteins separate the space and then act as the segmentation space where TiO_2 nucleates. With the growth of TiO_2, the organic template become thinner and finally invisible, and the porous TiO_2 network is formed. The observations here provide a direct and strong evidence for the well-known hypothesis, which proposed that the organic matrices act as "templates" for the mineral-formation during the biomineralization.[9]

To confirm the constituent nano-units of the MNT samples prepared with EPF proteins, transmission electron microscopy (TEM) was employed. A typical TEM image of the MNT-600 sample reveals the internal porosity of particles, which preliminarily shows the existence of evenly distributed pores inside the wall (Fig. 1g). The related selected area electron diffraction (SAED) exhibits diffraction rings corresponding to the anatase phase. A careful HRTEM image of the particle confirms its polycrystalline nature (Fig. 1h). The clear lattice fringes can be well assigned to the (101) pacing of anatase, which is in good agreement with the SAED pattern. The tiny nanocrystals are about 10~15 nm, further indicating that the walls are composed of nanocrystals subunits. Therefore, it could be found that the living EPF proteins not only act as "templates" for inducing the crystal formation, but also directs the assembly of nanoscale particles to form hierarchical structure. Recent studies have shown that the hierarchically porous structure may improve photocatalytic activity.[31,32]

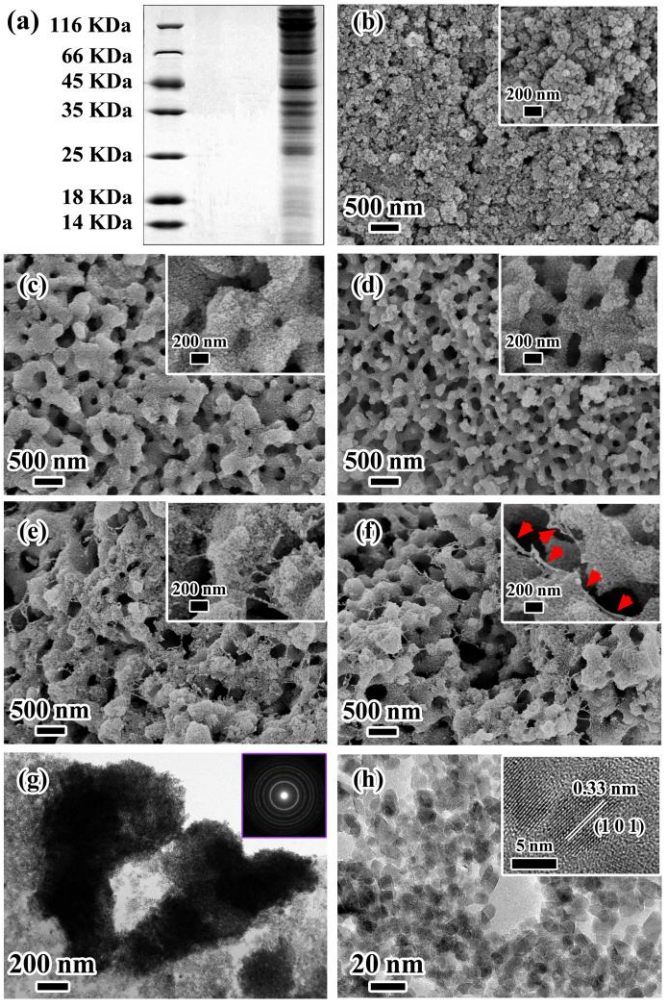

Fig. 1 (a) Natural composite EPF proteins were detected by 10% SDS-PAGE: left lane: molecular weight marker; right lane: EPF proteins. (b) SEM image of TiO_2 prepared with H_2O (pristine TiO_2). (c-f) SEM images of the TiO_2 sample prepared with different concentrations of EFP proteins at 150 °C for 12 h. (c) 300 μg/ml, (d) 600 μg/ml, (e) 900 μg/ml, (f) 1200 μg/ml. (g) TEM micrograph of MNT-600, the SAED pattern related to the particles shown in g. The diffraction rings from the centre are assigned to the (101), (004), (200), (211) and (204) planes of anatase. (h) HRTEM image of MNT-600 particles.

It is notable that hierarchically porous TiO_2 could also be prepared by the addition of TBT to pure water without any additive.[31,33] The as-prepared TiO_2 exhibited macroporous channels of ca. 3-5 μm (width) and ca. 60 μm (length) in

dimension, and the component TiO_2 particles with sizes from 300 to 500 nm, which were more than ten times larger than those of our products. Such distinct differences may be due to the following factors: (1) The special structure of MNT powders was directed by natural composite protein at molecular level other than self-assembly in alkoxide-water solutions; (2) The protein or pure water was dropwise added to TBT, which was adverse order compared to the previous reported methods. Thus, even in only pure water, no similar macroporous channels were obtained in our experiment.

X-ray diffraction was performed to investigate the effects of EPF proteins on the crystalline phases of TiO_2 samples (Fig. 2). Without protein, the pristine TiO_2 presents a main phase of anatase with small amount of brookite. The amount of brookite gradually decreases with the increase of protein concentration, suggesting that the EPF protein has controlled the crystalline phase and significantly prevented the formation of brookite. Simultaneously, the lower intensity and broader peaks of anatase are observed at higher concentrations. A rough estimation of crystallite size using the Scherrer formula is listed in Table 1. It can be clearly seen that the smaller crystallite size is achieved at the higher concentrations. Presumably, in the current situation, the contacts of TiO_2 grains are significantly limited by the hierarchical pores and residual proteins. Moreover, some atom impurities with the TiO_2, which may come from protein, could also slow the diffusion of ions necessary for rearrangement and grain growth.[36]

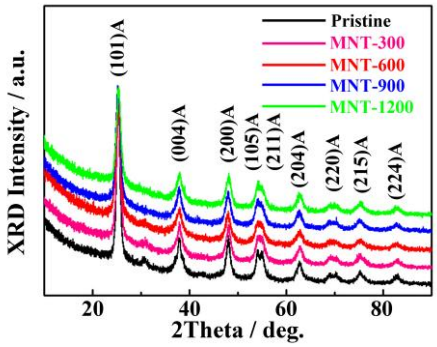

Fig. 2 X-ray diffraction patterns of pristine TiO_2 and MNT samples prepared with different EPF protein concentrations.

The porous structures of TiO_2 samples were also confirmed by the nitrogen adsorption-desorption measurement (Fig. 3a). The as-prepared TiO_2 samples show nitrogen sorption isotherms of type IV (BDDT classification).[24,37] For pristine TiO_2, a hysteresis loop is observed at a relative pressure range of 0.55-0.9, suggesting the presence of mesopores with narrow mouths (ink-bottles-like pores).[24] For MNT sample, hysteresis loops at high relative pressures are observed. Significantly, the hysteresis loop covers a relatively narrow range of relative pressures with typical span about 0.2 for MNT-300, which could be classified as a type-H1 hysteresis loop.[37] With the increased concentration of proteins, the hysteresis loops shift to lower relative pressure region, and the shapes of hysteresis loops evolve to H2.[37,38] Fig. 3b shows the corresponding pore size of samples calculated by the BJH method. The textural properties of all samples are also given in Table 1. It can be found that smaller average pore size is achieved at the higher concentration. Presumably, more natural proteins could lead to a denser organic framework, which provides more sites for TiO_2 nucleation and growth. Thus, high porosity but small pore size could be formed in TiO_2 samples.

Table 1 Effects of Protein Concentrations on Physicochemical Properties of TiO_2 Samples

Sample	Phase	Crystallite size[c] [nm]	S_{BET} [m^2 g^{-1}]	Pore volume [cm^3 g^{-1}]	Pore size [nm]
Pristine	A[a]/B[b]	20.1	123	0.38	8.8
MNT-300	A/B (trace)	15.2	116	0.37	11.7
MNT-600	A	12.9	126	0.40	10.1
MNT-900	A	10.5	168	0.40	7.5
MNT-1200	A	9.2	178	0.42	7.4

[a] A denotes anatase. [b] B denotes brookite. [c] Crystallite size is determined by the broadening of TiO_2 (101) facet diffraction peak using the Scherrer formula.

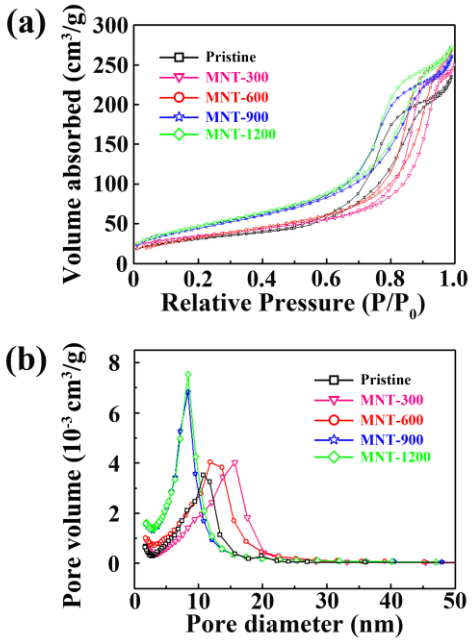

Fig. 3 (a) N_2 adsorption-desorption isotherms and (b) the pore size distribution of pristine TiO_2 and MNT samples.

The surface chemical bonding of MNT sample has also changed, as shown by XPS in Fig. 4. Here we take MNT-600 sample as an example. Before being tested, the sample were pre-treated by a typical chemical method of immersing powders in the aqueous solution consisting of 6M GuHCl and

1% SDS at 37 °C for 12 h, and the residual proteins in product were successfully eliminated.[39] The XPS survey shows the sample contains Ti, O, and C elements. Besides, weak nitrogen peak is also present in the sample (Fig. 4a). The C1*s* peak at 284.6 eV is always attributed to the contaminants in the preparation or test process. Moreover, the atomic concentration of N has been calculated based on XPS data. The result suggests that 0.48 at% N has been doped into the MNT-600 sample. As seen in Fig. 4b, two peaks corresponding to Ti2$p_{3/2}$ and Ti2$p_{1/2}$ were observed at 458.5 and 464.4 eV, respectively, which are attributed to the characteristic peaks of Ti^{4+} on the surface of TiO_2.[26] Fig. 4c shows the O1*s* XPS spectra. The O1*s* peak can be resolved into three peaks at 529.6, 531.1 and 532.2 eV. The peak at 529.6 eV is the characteristic of the lattice oxygen of TiO_2, and the rest two peaks are ascribed to Ti-OH species.[26,40] Fig. 4d shows the N1*s* XPS spectra and a peak at about 400.1 eV is observed. It is well known that nitrogen can be located in the anatase lattice interstitially or/and substitutionally. As reported,[41] the N1*s* peak at ~400 eV is typically ascribed to the interstitial nitrogen dopant, while the peak at ~396 eV is owing to the substitutional nitrogen dopant. Therefore, it is conceivable that the natural EPF protein presents unique affinities toward TiO_2 and acts as sources for interstitial nitrogen doping.

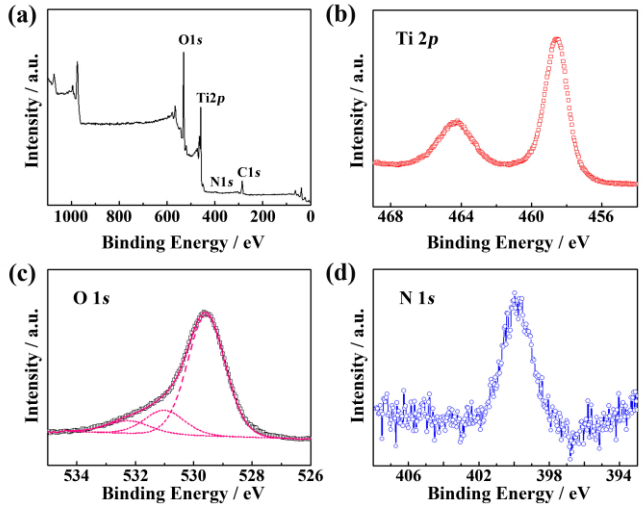

Fig. 4 XPS spectrum of the MNT-600 sample: (a) survey XPS; (b) Ti2*p*; (c) O1*s*, the black curve is XPS data, and the pink curves are the fitting of experimental data; (d) N1*s*.

Fig. 5a reports valence band (VB) XPS of reference (pristine) and MNT-600 sample. The pristine TiO_2 displays typical valance band DOS, with the band edge at ~1.26 eV below the Fermi energy.[40] However, the valance band of MNT-600 shows notable difference: the maximum energy associated with the band tail blue-shifted further toward the vacuum level at about 0.5 eV.[21] The shift of band gap is probably due to nitrogen impurities. It is assumed that the N atoms from the amino groups closely approach to the mineralized TiO_2, where it could be incorporated in the TiO_2 structure at low temperature. The band gap has been modified by the interstitial nitrogen doping, which extends the light absorption to the visible-light region (Fig. 5b).

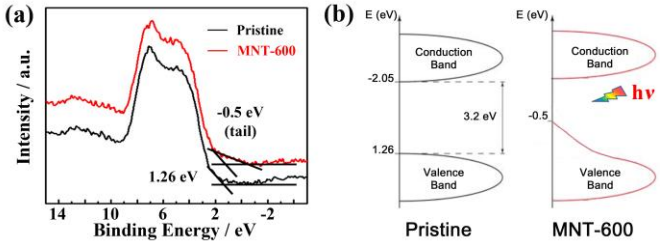

Fig. 5 (a) Valance-band (VB) XPS spectra and (b) Schematic of VB density of states for the pristine TiO_2 and MNT-600 sample.

During mineralization, the morphology and chemical state of TiO_2 are regulated by the biomacromolecules in natural living EPF proteins. On the basis of the experimental data, a tentative mechanism for the formation of 3D network structured N-TiO_2 was proposed, as illustrated in Fig. 6. In this case, when the EFP proteins were added into TBT, it is hypothesized that some positively charged proteins interact with the negatively charged TBT based on electrostatic interaction, resulting in the Ti-protein complex precursor. The morphology of as-synthesized Ti-protein precursor was investigated. As shown in Fig. 7, it could be found that the organic matrix assembles into the ordered linear arrays and then forms network structure on the nanometer scale. Du et. al has proposed that the self-assembly process of protein could take place *in vitro*, without requiring the corresponding cell.[12] The obtained matrix then acts as a nucleus center as well as a mechanistic framework to direct TiO_2 formation. The surface of organic template contains a large number of carboxyl groups and dangling amine to exchange ligands with titanium alkoxide. This effect ensures the hydrolysis occurring on the surface of template. Hence, the initial amorphous TiO_2 grains are assembled on the surface of framework to construct the network morphology, which is also evidenced by the structure of Ti-protein precursor (Fig. 7b). During the hydrothermal process, a controlled phase transition of amorphous-to-anatase occurs, accompanied by a moderate increase in the size. As for nitrogen doping, it has been demonstrated that when the crystal growth proceeds around structure-directing proteins, some N atoms of proteins or NOx products will interact with TiO_2,[42] leading to the formation of interstitial nitrogen at low temperature. On the other hand, natural proteins may further degrade and produce ammonia, phenols, indoles and amines *in vitro*. It is well known that small biomolecules such as amine could also induce the occurrence of nitrogen doping at low, or even room temperature.[43,44]

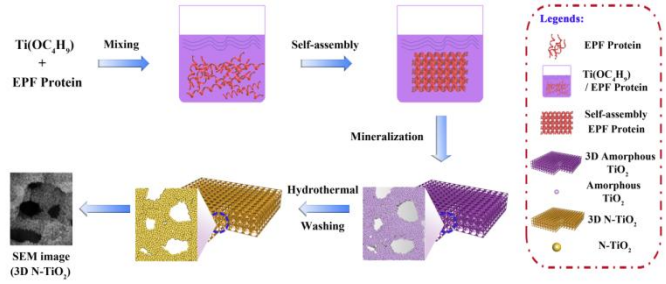

Fig. 6 Schematic of a tentative mechanism for the formation of 3D Network structured N-TiO_2.

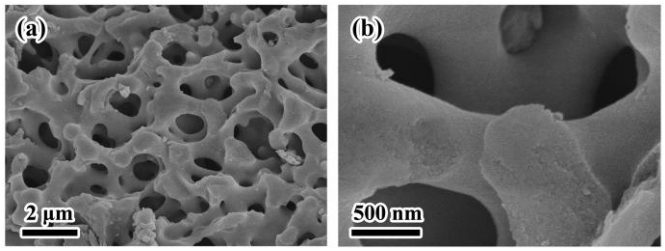

Fig. 7 (a) Overall view and (b) higher magnification of SEM images of Ti-protein precursor after mineralization of TBT in natural EPF protein for 4 h.

Since the natural EPF proteins have induced the hierarchically porous structure of MNT samples, we also investigated whether the living proteins could play an important role on the photocatalytic activity of samples. Here we used the commercial P25 as a reference, which was commonly used as reference in other reports. Moreover, in order to demonstrate the unique functions of EPF proteins, we also used the BSA-TiO_2 prepared with 600 μg/ml bovine serum albumin as another reference. Fig. 8a shows the UV-visible spectra of all samples. The white pristine TiO_2 and P25 present no ability in absorbing visible radiation as expected. In contrast, MNT and BSA-TiO_2 samples absorb the light from the UV to the visible range due to the nitrogen doping. As seen from Fig. 8b, the MNT samples show far superior visible-light photocatalytic activities on RhB degradation. The MNT-600 sample presents the highest photocatalytic activity, and the concentration of RhB is almost decreased by 100% just in 20 min. In comparison with other doped TiO_2 reported in previous studies[24-26,28,29,37,45,46] (as shown in Table 2), the obtained TiO_2 material shows an significant improvement on the visible-light photocatalytic activity. It clearly confirms that living EPF proteins could also regulate the functional property of TiO_2. The highest photocatalytic activity may be owing to the best balance among the hierarchical porosity, nitrogen content and amount of residual protein. Obviously, when the protein concentration continues to increase, the MNT samples exhibit poor photocatalytic activity for the lower crystallinity and more residual proteins. During five photodegradation cycles of RhB on the MNT-600 sample (Fig. 8c), the photocatalytic activity did not show any significant loss, thus indicating that the obtained TiO_2 is relatively stable and do not corrode during the photocatalytic oxidation of pollutant molecules. In order to eliminate the self-sensitized degradation effect of RhB,[47] the phenol degradation was also tested. With the MNT-600 as catalyst, the degradation of phenol with high concentration (1 mM) is almost completed in a short time of 5 h (Fig. 8d), however, the BSA-TiO_2 show much poorer photocatalytic activity. Thus, it could be concluded that the living EPF protein exhibit higher efficiency in improving the photocatalytic properties of materials owing to the synergistic effect of composite proteins, as compared with single protein or synthetic analogues.

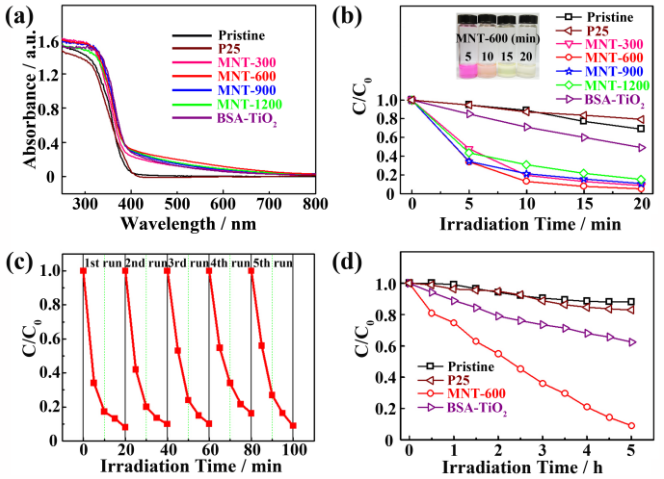

Fig. 8 (a) UV-vis absorption spectra of the pristine TiO_2, BSA-TiO_2 and MNT samples. (b) Comparison of the visible-light photocatalytic activity for the pristine, P25, BSA-TiO_2 and MNT samples on the degradation of 0.01 mM RhB. (c) Cycling tests of visible-light photocatalytic activity (RhB decomposition) of the MNT-600 sample. (d) Comparison of the visible-light photocatalytic activity for the pristine TiO_2, P25, BSA-TiO_2 and MNT-600 sample on the degradation of 1 mM phenol.

We also test the hydrogen evolution of TiO_2 samples from water splitting under visible-light irradiation. As shown in Fig. 9, no hydrogen evolution is observed due to the relatively large band gap of pristine TiO_2. With BSA-TiO_2 or MNT samples as photocatalyts, the rates of H_2 production are enhanced reflecting the activity of the extended tails or interstitial gap states of nitrogen.[40] The concentration of protein also has an impact effect on the H_2 evolution. When the concentration is 600 μg/ml, the average H_2-production rate reaches the highest value of 110 $\mu mol^{-1} \cdot g^{-1} \cdot h^{-1}$, leading to about 2-fold improvement in hydrogen evolution compared to the BSA-TiO_2. So the improvement of hydrogen production has been achieved by using natural living EPF proteins at low temperature. A decrease in H_2 production rate occurs with a continuous increase of protein concentration. Particularly, when the concentration rises up to 1200 μg/ml, the H_2-production rate sharply drops to 23 $\mu mol^{-1} \cdot g^{-1} \cdot h^{-1}$.

Journal of Materials Chemistry A

ARTICLE

Table 2 Comparison of the photocatalytic performances on degradation of RhB with other doped TiO_2 reported previously

Photocatalysis type	Dopant sources	Photocatalysis content (g/dm^3)	Initial RhB concentration (mol/dm^3)	Experiment conditions	RhB degradation	Ref
N-TiO_2	**EPF proteins**	**1**	**0.01**	**350 W Xe lamp; λ>420 nm**	**95%; 20 min**	**This work**
TiO_2-xNx	Urea	0.2	0.01	40W tungsten bulb; λ: 400~2500 nm	50%; 120 min	24
N-TiO_2	Urea	-	0.005	15 W, maximum intensity at 440 nm	60%; 220 min	25
N-TiO_2	Ethanediamine	1	0.02	300 W Xe lamp; λ>420 nm	87.16 %; 180 min	26
N-TiO_2	ammonia water	2	0.01	350 W Xe lamp; λ>420 nm	70%; 120 min	28
N-TiO_2	ammonia water	2	0.02	350 W Xe lamp; simulated sunlight irradiation	93.02% 120min	29
F/N–TiO_2	ammonium bifluoride	4	0.01	350 W Xe lamp; λ>400 nm	100%; 120 min	37
B/C-TiO_2	$BMIM^+$ BF4-	2	0.01	350 W Xe lamp; λ>420 nm	100% 120 min	28
Ag@TiO_2 core–shell	$AgNO_3$	2.5	0.01	300 W Xenon lamp	100%; 60 min	45
Ti^{3+}/TiO_2	Ti foil	1	0.02	300 W Xe lamp; λ>420 nm	41%; 240 min	46

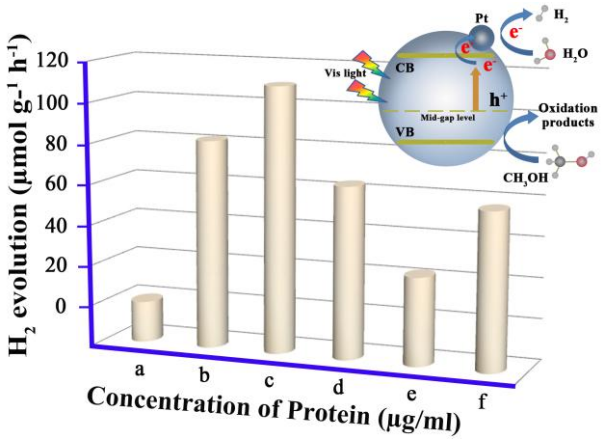

Fig. 9 Hydrogen evolution through photocatalytic water splitting with TiO_2 samples under visible-light irradiation.

On the basis of the above results, a tentative mechanism of the photocatalytic hydrogen production reaction is proposed (Fig. 9). Under visible-light irradiation, owing to the interstitial gap on the top of the O2*p* valance band, the photogenerated electrons of TiO_2 quickly transfer from the interstitial mid-gap to the CB of TiO_2, leaving holes in the original mid-gap and eventually dispersing to the surface of the macroporous walls of the 3D networked photocatalysts. The electrons accumulate on the Pt nanoparticles and then effectively react with the adsorbed H_2O to produce H_2, while holes react with methanol as a sacrificial reagent.[48,49] Since the large surface areas can be achieved by the hierarchically macro-/mesoporous structure, it can act as an electron collector and transporter to inhibit the recombination of electrons and holes, and also provide more opportunities for the charges to participate in the reactions. Moreover, the inter-connected macroporous network might facilitate mass transfer and lead to easy accessibility of active sites for the reactant molecules.[26,50] This is also the reason why MNT samples exhibit significantly enhanced photocatalytic activity on the degradation of organic pollutes.

To support and extend the current research, we investigated the functions of EPF proteins extracted from the same species of mussels (*Cristaria plicata*), but lived in different original areas. The natural proteins, which are extracted from one specified area of the same species, are generally considered to have much similarity on structure and function. Interestingly, it is found that the three similar EPF proteins have dramatically different effects on the functional property of TiO_2. As shown in Fig. 10, the MNT-600 exhibits the best visible-light photocatalytic activity on degradation of RhB. Moreover, the MNT-600 sample results in about 4-fold improvement on H_2 evolution than MNT-600-A, and 3-fold than MNT-600-B. The results strongly demonstrate that there are some mysterious relations between natural living proteins and functional properties of materials, which is undiscovered by us. The natural protein controls the TiO_2 formation in a sophisticated manner, and the characteristic of protein is decisive in determining the functional property of as-synthesized material. Unfortunately, the reasons why these similar proteins induce different properties of TiO_2 are still unclear. Thus, a series of systematic studies should be done in the future.

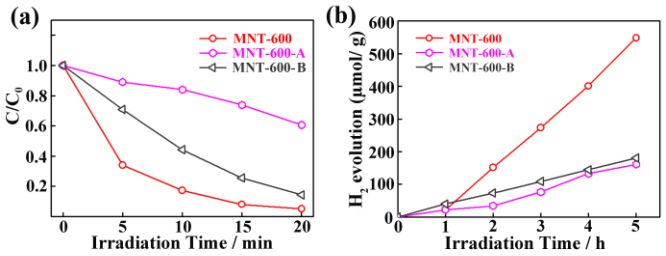

Fig. 10 Comparison of the visible-light photocatalytic activity for the TiO_2 samples on the (a) RhB decomposition and (b) hydrogen evolution. The samples were synthesized by using natural EPF proteins extracted from mussels lived in different areas.

4. Conclusions

Hierarchically macro-/mesoporous N-doped TiO_2 was fabricated by a bio-process inspired method that enabled simultaneous control of microstructure, crystal phase and light-use efficiency in a single process. During the crystallization, the morphology and crystal phase of TiO_2 was controlled by natural EPF proteins via the so-called 'template effect'. Moreover, nitrogen from the amino groups closely approached to the mineralized TiO_2, where it could be incorporated in the TiO_2 structure at low temperature. The results show that the TiO_2 samples exhibit significantly enhanced visible-light photocatalytic activities both in chemical waste remediation and hydrogen generation. It has been also found that EPF proteins, extracted from the same species of mussels but lived in different areas, show dramatically different effects on the photocatalytic properties of TiO_2. Therefore, we uncovered the mysterious relations between natural proteins and functional properties of materials, which doubtless evokes scientists to revaluate the effects of natural proteins on the functional properties, and also opens an avenue to produce advanced materials with optimized functional properties.

Acknowledgements

We thank S. H. Xie (Shao He Pear Company of Guang Dong province) kindly providing the living mussels and supporting field experiments; J. G. Yu and Yu Li (Wuhan University of Technology) for their help on the photocatalytic experiments and discussions. Financial support from National Natural Science Foundation of China (51521001) and Ministry of Science and Technology of China (2015DFR50650) are gratefully acknowledged. The Fundamental Research Funds for the Central Universities (WHUT, 2013-Ia-037 and 2013-YB-019) is also acknowledged.

Notes and references

[a]State Key Laboratory of Advanced Technology for Materials Synthesis and Processing, Wuhan University of Technology, Wuhan, 430070, China. E-mail: zyfu@whut.edu.cn (Z.-Y. Fu).
[b]School of Chemistry, Chemical Engineering, and Life Science, Wuhan University of Technology, Wuhan, 430070, China.
[c]Laboratory of Inorganic Materials Chemistry, University of Namur, B-5000 Namur, Belgium.

1. S. Weiner and H. D Wagner, *Annu. Rev. Mater. Sci*., 1998, **28**, 271-298.
2. L. Addadi, D. Joester, F. Nudelman and S. Weiner, *Chem. Eur. J*, 2006, **12**, 980-987.
3. V. C. Sundar, A. D. Yablon, J. L. Grazul, M. Ilan and J. Aizenberg, *Nature*, 2003, **424**, 899-900.
4. Y. Politi, T. Arad, E. Klein, S. Weiner and L. Addadi, *Science*, 2004, **306**, 1161-1164.
5. H. A. Lowenstam and S. Weiner, *On Biomineralisation*, Oxford Univ. Press: New York, 1989.
6. S. Mann, *Biomineralization*, Oxford Univ. Press: Oxford, 2001.
7. W. D. Kingery, *Introduction to Ceramics*, John Wiley & Sons: New York, 1960.
8. M. Cusack and A. Free, *Chem. Rev.*, 2008, **108**, 4433-4454.
9. S. Weine and W. Traub, *Phil Trans R Soc Lond B.,* 1984, **304**, 425-434.
10. M. B. Dickerson, K. H. Sandhage and R. R. Naik, *Chem. Rev.*, 2008, **108**, 4935-4978.
11. L. B. Gower, *Chem. Rev.*, 2008, **108**, 4551-4627.
12. C. Du, F. Falini, S. Fermani, C. Abbott and J. Moradian-Oldak, *Science*, 2005, **307**, 1450-1454.
13. F. Marin, G. Luquet, B. Marie, D. Medakovic, *Curr Top Dev Biol.*, 2008, **80**, 209-276.
14. W. J. Lee, J. M. Lee, S. T. Kochuveedu, T. H. Han, H. Y. Jeong, M. Park, J. M. Yun, J. Kwon, K. No, D. H. Kim and S. O. Kim, *ACS Nano*, 2012, **6**, 935-943.
15. T. Nonoyama, T. Kinoshita, M. Higuchi, K. Nagata, M. Tanaka, K. Sato and K. Kato, *J. Am. Chem. Soc.*, 2012, **134**, 8841-8847.
16. J. Miot, N. Recham, D. Larcher, F. Guyot, J. Brest and J.-M. Tarascon, *Energ y Environ. Sci.*, 2014, **7**, 451-460.
17. J. G. Yu, L. F. Qi and M. Jaroniec, *J. Phys. Chem. C*, 2010, **114**, 13118-13125.
18. R. W. Mo, Z. Y. Lei and K. N. Sun, *Adv. Mater.*, 2014, **26**, 2084-2088.
19. T. Kamegawa, Y. Ishiguro, H Seto and H. Yamashita, *J. Mater. Chem. A,* 2015, **3**, 2323-2330.
20. J. Wang, D. N. Tafen, J. P. Lewis, Z. L. Hong, A. Manivannan, M. Zhi, M. Li and N. Q. Wu, *J. Am. Chem. Soc.*, 2009, **131**, 12290-12297.
21. A. Naldoni, M. Allieta, S. Santangelo, M. Marelli, F. Fabbri, S. Cappelli, C. L. Bianchi, R. Psaro and V. D. Santo, *J. Am. Chem. Soc*., 2012, **134**, 7600-7603.
22. D. Fan, G. Sen, H. Q. Wang, X. F. Li, Z. B. Wu, *J. Phys. Chem. C*, 2011, **115**, 13285-13292.
23. X. Chao, Wang T, Yang G, Y. Bolun and S. Ding, *J. Mater. Chem. A,* 2014, **2**, 7674-7679.
24. G. S. Shao, X. J. Zhang and Z. Y. Yuan, *Appl. Catal., B: Environ.*, 2008, **8**, 208-218
25. G. B. Soares, B. Bravin, C. M. P. Vaz and C. Ribeiro, *Appl. Catal., B: Environ.*, 2011, **106**, 287-294.
26. T. Wang, X. Q. Yan, S. S Zhao, B. Lin, C. Xue, G. D. Yang, S. J. Ding, B. L. Yang, C. S. Ma, G. Yang and G. R. Yang, *J. Mater. Chem. A*, 2014, **2**,15611-15619.
27. G. D. Yang, Z. Jiang, H. H. Shi, T. C. Xiao, Z. F. Yan, *J. Mater. Chem. A*, 2010, **20**, 5301-5309.
28. J. G. Yu, Q. Li, S. W. Liu and M. Jaroniec, *Chem. Eur. J.* 2013, **19**, 2433-2441.
29. X. W. Cheng, X. J. Yu and Z. P. Xing, *Appl. Surf. Sci.*, 2013, **268**, 204-208.
30. J. N. Xu, P. Sun, X. Zhang, P. Jiang, W. B. Cao, P. W. Chen and H. B. Jin, *Mater. Manuf. Processes*, 2014, **29**, 1162-1167.
31. Y. Li, Z. Y. Fu and B. L. Su, *Adv. Funct. Mater.*, 2012, **22**, 4634-4667.
32. D. R. Rolison, *Science*, 2003, **299**, 1698-1701.
33. J. G. Yu, Y. R. Su and B. Cheng, *Adv. Funct. Mater.*, 2007, **17**, 1984-1990.
34. J. F. Ye, W. Liu, J. G. Cai, S. Chen, X. W. Zhao, H. H. Zhou and L. M. Qi, *J. Am. Chem. Soc.*, 2011, **133**, 933-940.
35. M. Awaji and Machii, *Aqua-Bio Science Monographs*, 2011, **4**, 1-39.
36. J. L. Sumerel, W. J. Yang, D. Kisailus, J. C. Weaver, J. H. Choi and D. E. Morse, *Chem. Mater.*, 2003, **15**, 4804-4809.
37. S. W. Liu, J. G. Yu and W. G. Wang, *Phys. Chem. Chem. Phys.*, 2010, **12**, 12308-12315.
38. K. S. W. Sing, D. H. Everett, R. A. W. Haul, L. Moscou, R. A. Pierotti, J. Rouquerol and T. Siemieniewska, *Pure Appl. Chem.*, 1985, **57**, 603.
39. L. Kurth and P. J. Rogers, *J. Food Sci.*, 1984, **49**, 573-576.
40. X. B. Chen, L. Liu, P. Y. Yu and S. S. Mao, *Science*, 2011, **331**, 746-750.
41. A. Fujishima, X. T. Zhang and D. A. Tryk, *Surf. Sci. Rep.*, 2008, **63**, 515-582.
42. C. D. Valentin, E. Finazzi, G. Pacchioni, A. Selloni, S Livraghi, M. C. Paganini and E. Giamello, *Chem. Phys.*, 2007, **339**, 44-56.
43. C. Burda, Y. B. Lou, X. B. Chen, A. C. S. Samia, J. Stout and J. L. Gole, Nano Lett., 2003, 3, 1049-1051.
44. H. Han, and R. Bai, Ind. Eng. Chem. Res., 2009, 48, 2891-2898.
45. B. Cheng, Y. Le and J. G. Yu, *J. Hazard. Mater.*, 2010, **177**, 971-977.
46. G. S. Li, Z. C. Lian, X. Li, Y. Y. Xu, W. C. Wang, D. Q. Zhang, F. H. Tian and H. X. Li, *J. Mater. Chem. A*, 2015, **3**, 3748-3756.
47. W. Zhao, C. C. Chen, W. H. Ma, J. C. Zhao, D. X. Wang, H. Hidaka and N. Serpone, *Chem. Eur. J*, 2003, **9**, 3292-3299.
48. J. G. Yu, L. F. Qi and M. Jaroniec, *J. Phys. Chem. C*, 2010, **114**, 13118-13125.
49. L. Ge, C. C. Han, X. L. Xiao and L. L. Guo, *Int. J. Hydrogen Energy*, 2013, **38**, 6960-6969.
50. T. Dogu, *Ind. Eng. Chem. Res*., 1998, **37**, 2158-2171.